J Mater Sci: Mater Electron (2016) 27:1693–1699
DOI 10.1007/s10854-015-3941-z

Controllable preparation of 2D and 3D ZnO micro-nanostructures and their photoelectric conversion efficiency

Luyue Yang[1] · Yi Zhou[1] · Jun Lu[1] · Chaocheng Li[1] · Yuhuan Liu[1] · Yiwei Wu[1] · Mengyao Li[1]

Received: 2 August 2015 / Accepted: 20 October 2015 / Published online: 26 October 2015

Abstract The different morphological ZnO micro-nanostructures were prepared by solvothermal method and their photoelectric conversion efficiency applied in dye-sensitised solar cells (DSSCs) were be analysed. The morphologies and crystalline structures of the ZnO nanocrystals grown under different driving forces, which were characterised by scanning electron microscopy, transmission electron microscopy and X-ray diffraction measurements. The results showed that different additives caused different growing directions for the crystal plane and then formed ZnO micro-nanostructures with different morphologies. The UV–visible diffuse reflectance spectra displayed that nanorod-assembled 3D urchin-like ZnO had the strongest absorbance intensity. When they were used as photo-anodes for DSSCs, the I–V curve showed their photoelectric conversion efficiency enhanced to different degrees. The highest was that of the nanorod-assembled 3D urchin-like ZnO micro-superstructures, which was synthesised under $NaBH_4$ and 25 % concentrated aqueous ammonia reaction system. Its photoelectric conversion efficiency is 2.37 %. Other hand, this simple and controlled method is promising to prepare the low-cost, environmentally friendly and high performance innovative structural materials.

✉ Yi Zhou
zhouyihn@aliyun.com; zhouyihn@163.com

[1] Department of Chemistry and Biological Engineering, Changsha University of Science and Technology, Changsha 410114, China

1 Introduction

With the energy demand increasing, the research of solar-energy-driven optoelectronic nano-semiconductor materials becomes promising. The 3D ZnO semiconductor micro-nanostructures, as semiconductor materials, exhibit the quantum-range size and surface-interface effects that are unique among nanomaterials. They show characteristic features like optical, photocatalytic, electrical, non-toxic and non-migratory properties that broaden their scope of applications [1], such as in antibacterial deodorisation, disinfection and photocatalysis. They are also used in gas sensors and as materials for piezoelectric, coating, dye-sensitised solar cell (DSSC) devices and in other applications [2, 3]. Dianyi Liu et al. [4] reported that, when ZnO nanostructures are used as the electron transport layer of a $CH_3NH_3PbI_3$–perovskite-based solar cell at room temperature, the photoelectric conversion efficiency can reach 15.7 %. This solar cell was listed in a science magazine as one of the ten scientific and technological breakthroughs in 2013. Hence, more and more researchers take keen interest to the synthesis of 3D ZnO micro-nanostructure materials with 1D or 2D structures as assembly structures because of special morphology (porosity) and high specific surface area [5, 6]. Seho Oh et al. [1] prepared spherical and rod-shaped ZnO nanoparticles by modified sol–gel methods, and they found that the rod-shaped ZnO particles exhibit higher photoelectric conversion efficiency. Qun Ma and Jinlei Xu et al. [7, 8] synthesised ZnO micro-flowers by a simple solution deposition method. As they found, the nanocrystals showed higher light harvesting efficiency in comparison to that of ZnO nanoparticles, and it may be tempting for further application. Arpita Jana et al. [9] reported that the energy conversion efficiency is closely related to the surface area of the ZnO structures. Therefore,

the synthesis of ZnO micro-nanomaterials with different morphologies are very important, especially the preparation of the 3D morphologies which combine with the unique properties of 1D or 2D structures. Different ZnO micro-nanostructures with various morphologies have been synthesised. These structures include 0D (quantum dots) [10], 1D (nanowires, nanorods, nanotubes) [11–13], 2D (nanoribbons, nanosheets) [5, 14] and 3D nanostructures (nanospheres, nano-flowers) [15, 16], as well as other nanostructures based on these structure types [17, 18]. However, assembling a stable, dense, porous, uniform, sea-urchin spherical-structured ZnO on a soft pattern still needs to be studied further. Therefore, the nanorod-assembled 3D urchin-like ZnO micro-superstructures are considerable in this work especially when applied in DSSCs. Given its large surface area, its capacity for dye adsorption and photo-generated electron production can be increased; hence, the photoelectric conversion efficiency can be improved [19–21]. Then, the ZnO micro-nanostructures with different morphologies have been synthesised through different methods, and their characteristics are dependent on the grown shapes. In addition, different reaction solvents provide different energy for crystal growth. At the same time, additives can be added to change the nanocrystal surface energy, which can guide the crystal growth and form different morphologies. Thereby, the synthesis of 3D micro-nanostructures with nano-pin ZnO and ZnO nanosheets is controlled. Their potentials are significantly higher than that of low-dimensional ZnO structures obtained previously [22]. Respectively, the simple and controlled preparation method is significant.

In this study, the effect of different additive environment on the growth of ZnO nanocrystals is considered in search of appropriate adjuvant-controlled synthesis of 3D crystalline ZnO. The photoelectric conversion efficiencies of the optical anodes formed by the different morphology nanostructures ZnO applied in DSSCs were studied. A simple and controlled method, using H_2 as the soft template, which preparing the nanorod-assembled three-dimensional urchin-like ZnO micro-superstructures was sought.

2 Experimental

2.1 Experimental procedure

FTO coated glass substrates were cleaned in the ultrasonic bath with acetone, ethanol and deionized water. In a typical procedure, 2 mmol $Zn(Ac)_2{\cdot}2H_2O$ were dissolved in a certain amount of deionized water under magnetic stirring to form a clear solution, firstly. Then slowly dropped 4 mol/L of NaOH (or 25 % $NH_3{\cdot}H_2O$) aqueous solution to produce precipitation, stirring and until the precipitate dissolved at room temperature. Added an equal amount of ethanol (volume ratio: 1:1), stirring continued until homogeneous. Finally, a certain quantity of additive (sodium citrate, $NaBH_4$ or their mixture), is added under stirring for 10–20 s, then the precursor solution was obtained.

Subsequently, the precursor solution was transferred to a Teflon-sealed autoclave, Then, to synthesise the ZnO micro-nanostructures, the reaction was performed at 120 °C for 6 h. After deposition, the samples were cleaned several times with double distilled water and absolute ethanol, and then dried in a vacuum oven at 60–70 °C for 4–6 h.

2.2 Construction of dye-sensitized solar cell

The obtained electrodes with different ZnO micro-nanostructures were dipped in a N3 solution (0.5 mmol/L in dry ethanol solution) for 12 h. Pt electrode was the counter electrode, which was obtained by coating with a drop of H_2PtC_{l6} solution (5 mmol/L in isopropanol solution) on FTO and heated at 300 °C for 15 min. A sandwich type cell was assembled with the dye-covered ZnO electrode and Pt-counter electrode. 0.5 mol/L KI, 0.05 mol/L I_2 in acetonitrile was the electrolyte solution [23].

2.3 Characterization

The samples were characterized using scanning electron microscopy (SEM, JEOL JSM-6700F), field emission transmission electron microscope (STEM, JEOL JEM-2100F) and X-ray diffraction system (SIEMENS D5000) operating at Cu Kα radiation (40 kV/40 mA) and the scan range was 20°–80°. The light scattering phenomenon were analyzed by the UV–visible diffuse reflectance spectroscopy (UV–Vis DRS) using a UV–Vis spectrophotometer (TU-1901, Beijing). The optical properties, including short-circuit current density, open-circuit voltage, fill factor and photoelectric conversion efficiency were measured by an electrochemical workstation (CHI 660D, ChenHua Instrument Co.).

3 Results and discussion

Different additives imply a significant effect on the micro-nanostructural ZnO formation. They provide a driving force for the ZnO crystal growth in different directions. And the ZnO nuclei gradually grow into nanorods with a diameter of ~100 nm only when $NaBH_4$ is added. As the reaction proceeds, the nanorods self-assemble into the flower-like ZnO micro-nanostructures (Fig. 1a). When

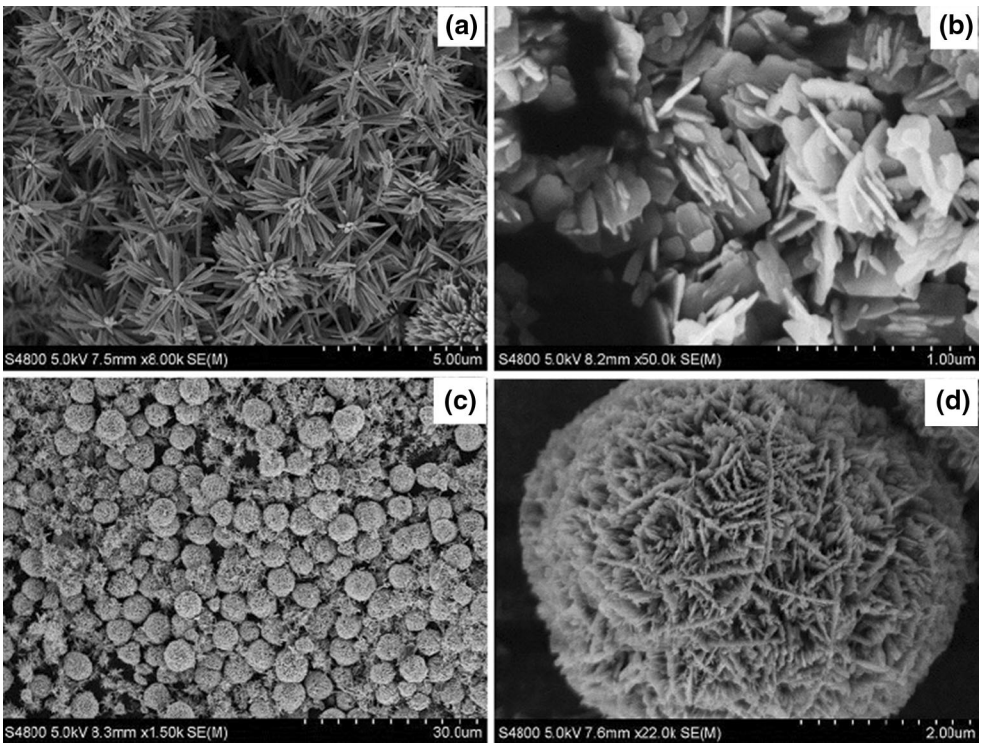

Fig. 1 SEM images of the ZnO micro-nanocrystalls synthesised by solvothermal method at the same experimental conditions: **a** 3D flower-like cone-bar ZnO synthesised in $NaBH_4$; **b** ZnO nano-sheets synthesised in sodium citrate; **c** nanosheet-assembled 3D spherical structure ZnO synthesised in sodium citrate and $NaBH_4$; **d** individual ZnO sphere at higher resolution

sodium citrate is used as adjuvant, the morphology changed. The most prominent change is that the nanorods converted into nanosheets, and new nanosheets grow on the nanosheets at an oblique angle; these nanosheets is approximately 20 nm thick (Fig. 1b). When $NaBH_4$ and sodium citrate are added (Fig. 1c), ZnO nano-spheroids composited of tiny nanosheets are synthesised. A certain porosity degree is observed between the sheets, and the spheroid diameters are $\sim$4 μm. Figure 1b is the same as Fig. 1c except that the latter shows high-resolution topography. Sodium citrate and $NaBH_4$ interact and provide a new driving force for the growth of ZnO nano-spheroids formed from the nanosheets in the same reaction system. Obviously, different adjuants provide the different effect for the growth of ZnO crystal nuclei in different directions. This phenomenon is further analysed with X-ray diffraction (XRD), as well be shown in Fig. 3.

The morphologies shown in Fig. 1b, c are preferable. The related SEM and TEM images are shown in Fig. 2, where the microscopic crystal orientation and morphology of the ZnO micro-nanostructures are shown. Figure 2a, b shows that the nanosheets, which are approximately 3.5 μm in diameter, are assembled into spheroids according to a certain pattern, and the spherical surface renders many large and small "pentagram" shapes. This phenomenon may be related to the nanosheets arrangement. The ZnO nano-spheroids have rough surfaces, and the sheet structures arranged on the surfaces are serrated. The TEM image of the typical nano-spheroid surface portion, as shown in Fig. 2c, proves that the nanosheet structures are superposed in a certain direction, and the mono-nanosheet surface is very thin and smooth. The high-resolution TEM (HRTEM) of the atomic phase region is shown in Fig. 2d. The structure clearly exhibits a lattice spacing of 0.281 nm, which corresponds to the distance between the two adjacent (0002) planes of ZnO. In brief, sodium citrate and $NaBH_4$ have a crucial effect on the ZnO nanocrystal growth orientations and can cause different ZnO structures and morphologies.

The XRD patterns of the ZnO nanocrystals with different morphologies are shown in Fig. 3. The diffraction peaks at $2\theta = 31.6°$, 34.3°, 36.2°, 47.5°, 56.5° and 62.7° correspond to wurtzite planes (100), (002), (101), (102), (110) and (103), and these values can be readily indexed to the hexagonal wurtzite phase of ZnO (JCPDS Card No. 36-1451). I. Beinik and G.Brauer et al. [24, 25] described the crystal structure of ZnO detailed by using XRD and AFM (atomic force microscopy). A comparison of the three patterns shown in Fig. 3 indicates that the growth of the (002) planes is weak. This finding may be due to the special environment caused by both sodium citrate and $NaBH_4$; they produce specific orientation of crystal growth.

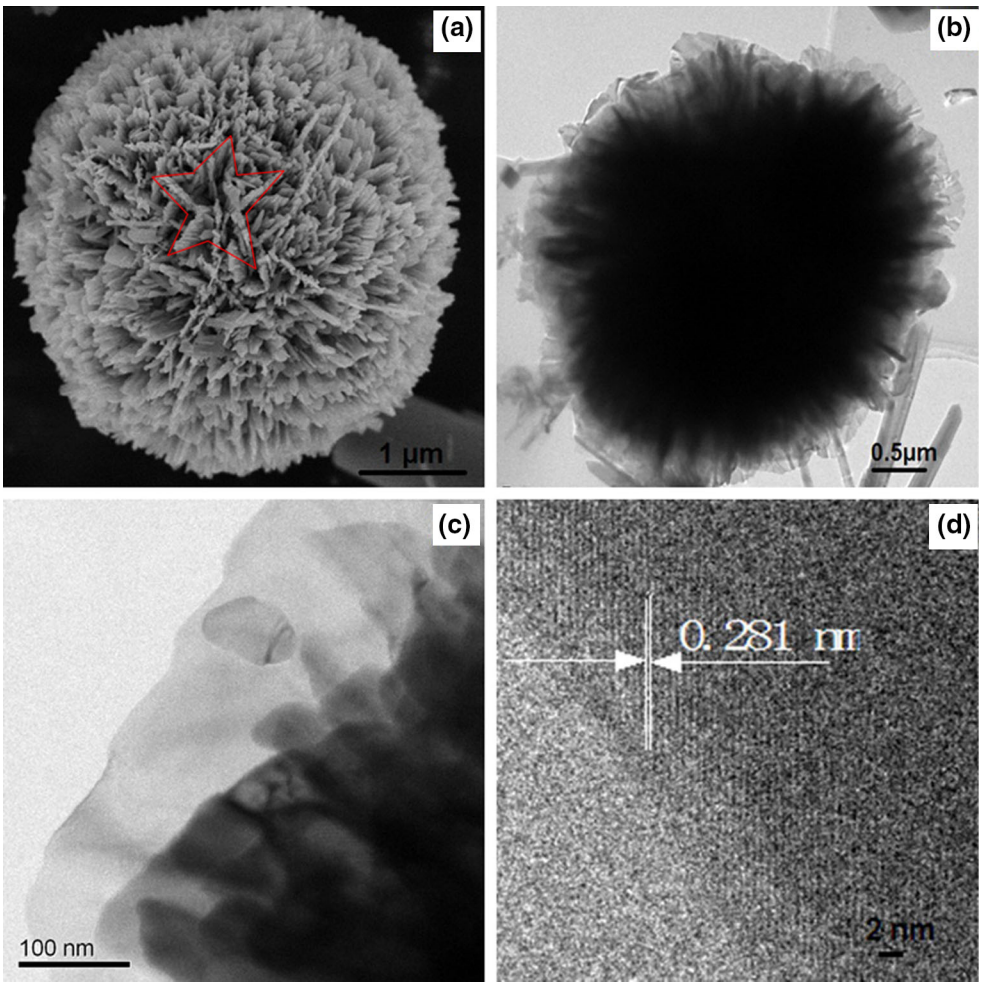

Fig. 2 Electron microscope images of nano-sheet assembled 3D spherical structure ZnO: **a** SEM image; **b** TEM image; **c** TEM image of nano-sheets; **d** High-resolution TEM lattice diagram

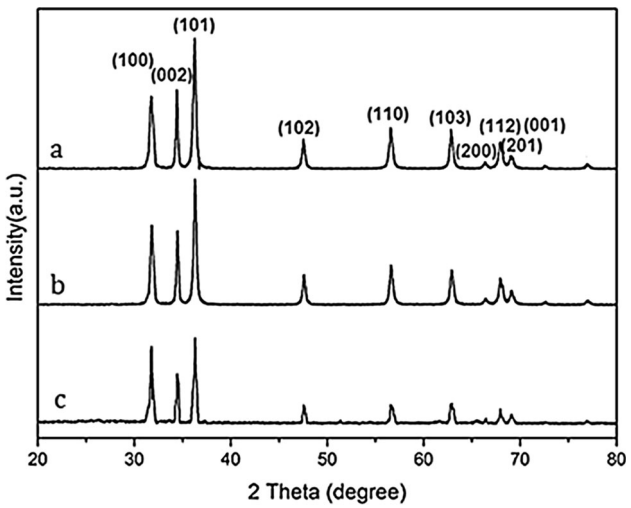

Fig. 3 XRD patterns of micro-nano crystalline ZnO: **a** 3D flower-like cone-bar ZnO synthesised in $NaBH_4$; **b** ZnO nano-sheets synthesised in sodium citrate; **c** nanosheet-assembled 3D spherical structure ZnO synthesised in sodium citrate and $NaBH_4$

Under normal circumstances, the ZnO crystal plane (001) grows swiftly with the formation of 1D ZnO rod. Given the action of the crystal growth rate and anisotropy under certain experimental conditions, the low growth rate gradually accelerated, and 3D spherical-structured ZnO nanosheets with special growth orientations are synthesised.

After optimisation of the experimental conditions with $NaBH_4$ as additive, 25 % concentrated aqueous ammonia reaction system, 120 °C temperature control and 3 h of reaction time, then 3D urchin-like ZnO micro-superstructures are synthesised from the nanorods, as shown in Fig. 4. The SEM and TEM images of the ZnO crystallite topography are shown in Fig. 4a, b, which reveal that the prepared 3D sea urchin-like ZnO is composed of several individually aligned nanorods, which radiate from the centre of the crystals with an appropriate tightness, and these nanorods are of uniform size. The cross-sectional SEM image, in the upper left of Fig. 4a, indicates thickness

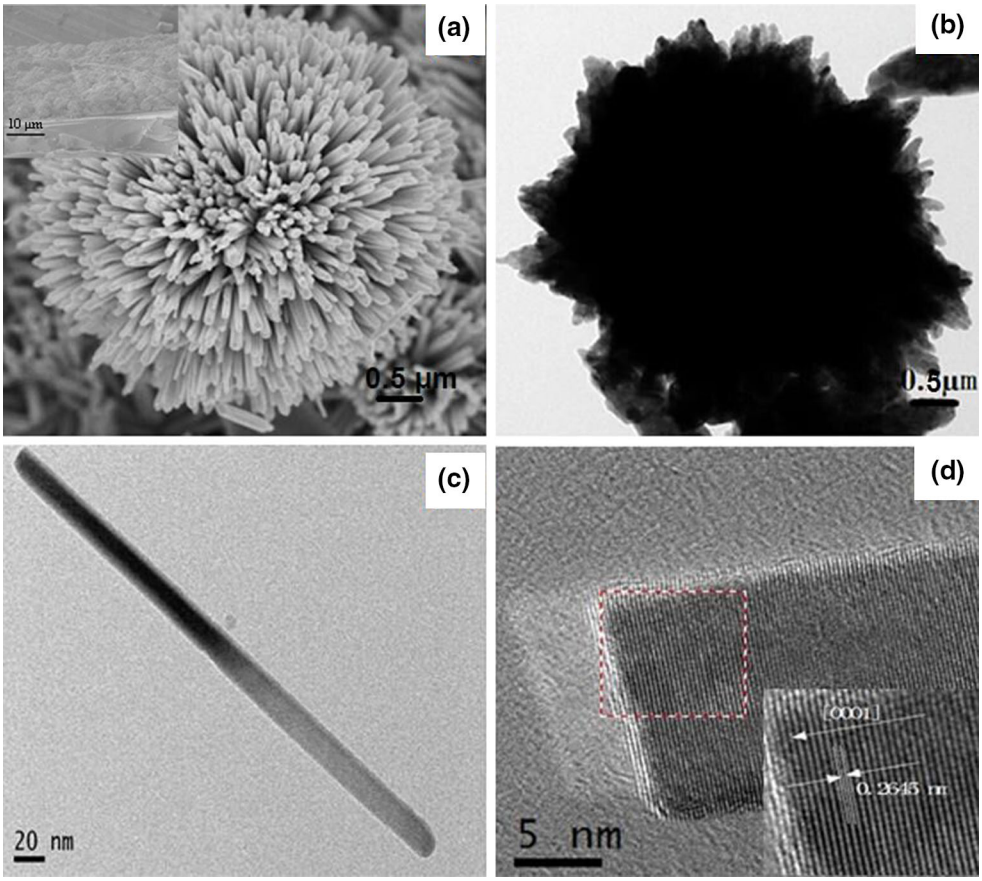

Fig. 4 Electron microscope images of nanorod-assembled 3D urchin-like ZnO: **a** SEM image and the cross-sectional SEM image; **b** TEM image; **c** TEM image of a single nanorod; **d** High-resolution TEM image

of the film is about 20 μm. The top surface of the urchin-ball nanorods is obviously rough and uneven. The rough and uneven interface would strengthen internal light scattering, and the larger crystallites, interface area also support the charge transport [26]. Figure 4c shows the detailed topography of a single nanorod. The ZnO nanorod surface is relatively smooth and has good orientation, with an average width of approximately 20 nm. The HRTEM image in Fig. 4d shows that the lattice spacing is approximately 0.2645 nm, which corresponds to the (002) planes of the hexagonal wurtzite ZnO, suggesting that the sample has a single-crystalline structure. This 3D structure is arranged orderly and can increase the transmission path of electrolytes; thus, it can be applied in DSSCs. In addition, the specific surface area and reaction centre are increased. Thus, the structure can effectively improve the photoelectric conversion efficiency [22].

In order to investigate the light absorption and scattering ability of different ZnO micro-nanostructures, the UV–visible diffuse reflectance spectra were measured, as shown in Fig. 5a. It certificated the nanorod-assembled 3D urchin-like ZnO had the highest absorption intensity. The enhanced absorption intensity may be related to the rules of the ordered arrangement of 3D urchin-like ZnO nano-rods, because of the light reflect back and forth among the nanorods. When the ZnO micro-nanostructures with different morphologies were synthesized with additives, the ZnO particles were applied as optical anode in DSSCs, and the photoelectric conversion efficiency was improved at different degrees. The corresponding parameters, including the short-circuit current density (J_{SC}), open-circuit voltage (V_{OC}), fill factor (FF) and photoelectric conversion efficiency (η), are listed in Table 1. When the DSSC optical anode is assembled with the 3D flower-like cone-bar ZnO synthesised in $NaBH_4$, the photoelectric conversion efficiency is minimum (Fig. 5b). This may be caused by a small surface area and low dye adsorption rate. The second is the 3D spherical structure ZnO that is synthesised with sodium citrate and $NaBH_4$. Its photoelectric conversion efficiency increased by 84.96 % compared with that of the flower-like cone-bar ZnO. As evident from Fig. 1, the formations possess high porocity, and the numerous pores of the 3D sphere surface further increase the surface area. It can absorb more dye, has more reactive centres and

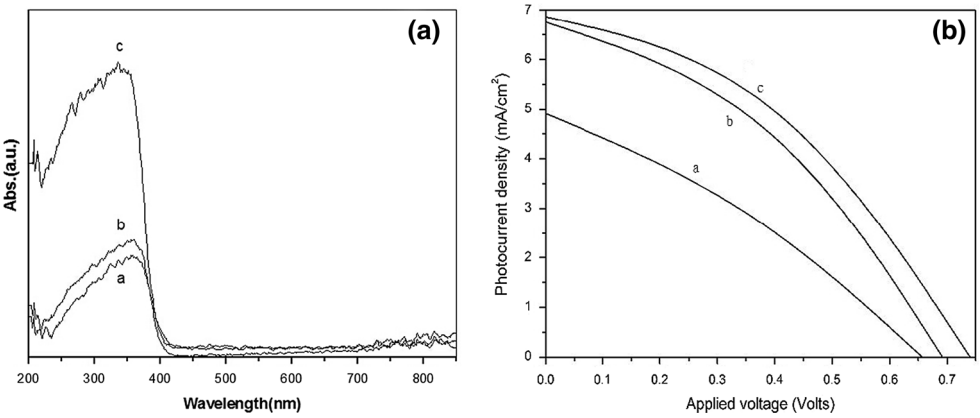

Fig. 5 **a** UV–visible diffuse reflectance spectra; **b** IV curves for the DSSCs assembled with different morphological ZnO micro-nanostructures: (*a*) 3D flower-like cone-bar ZnO; (*b*) nanosheet-assembled 3D spherical structure ZnO; (*c*) nanorod-assembled 3D urchin-like ZnO (the labelling is consistent with that of Fig. 1)

Table 1 Photoelectric properties parameters of different morphologies of ZnO nanostructures film applied on DSSCs

Film type	J_{SC} (mA/cm^2)	V_{OC} (V)	FF	η (%)
3D flower-like cone-bar ZnO	4.92	0.657	0.349	1.13 ± 0.04
Nanosheet-assembled 3D spherical structure ZnO	6.76	0.692	0.448	2.09 ± 0.13
Nanorod-assembled 3D urchin-like ZnO	6.87	0.740	0.466	2.37 ± 0.09

induces more photo-generated electrons. The relation between FF and η is:

$$\eta = \frac{P_m}{P_{in}} = \frac{I_{sc} \times V_{oc} \times FF}{P_{in}} \quad (1)$$

From (1), the η increases with the FF.

From Table 1, the values of J_{SC}, V_{OC}, FF, and η of the nanorod-assembled 3D urchin-like ZnO micro-superstructures are 6.87 mA/cm^2, 0.74 V, 0.466 and 2.37 %, respectively. Because the electronic transmission path nanosheet-assembled structure is poorer than the nanorod-assembled, the photoelectric conversion efficiency is maximal and increased by 13.4 % as compared with that of the 3D spherical-structured ZnO assembled from nanosheets. And it may be related to the further increase in surface area, reactivity centres, and higher light absorption intensity, thereby improving its effective electron transport paths. Meanwhile, a variety of surface effects and the quantum size effect caused by the large surface area also has a great impact on the optical properties of ZnO.

4 Conclusions

In summary, ZnO micro-nanostructures were synthesised in different adjuvant solvent systems (sodium citrate, $NaBH_4$ or both) by solvothermal method, and ZnO nanosheets, flower-like cone-bar ZnO, 3D spherical-structured ZnO assembled from nano-sheets were obtained, respectively. When the nanostructures were applied in DSSCs, different photoelectric properties were obtained. Furthermore, the optimised experimental condition, using the $NaBH_4$ and ammonia system, the synthesis of 3D urchin-like ZnO micro-superstructures with perfect crystallinity, uniform morphology with excellent denseness is obtained. It has rough and uneven surface, thus a larger surface area, mesoporous characteristics and more reactive centres, which can increase the dye adsorption rate and the number of generated carriers per unit time, thereby further improving the optical activity. The photoelectric conversion efficiency is the highest. Therefore, this work is envisioned to synthesise the multifunctional micro-nanostructures ZnO, and promote their practical applications in DSSCs, and even the environmental and other energy storage issues.

Acknowledgments This work was supported by the National Natural Science Foundation of China (Grant Nos. 21171027 and 51172031). The authors are also grateful to the aid provided by the Science and Technology Innovative Research Team in Higher Educational Institutions of Hunan Province.

References

1. S. Oh et al., Effect of ZnO nanoparticle morphology and post-treatment with zinc acetate on buffer layer in inverted organic photovoltaic cells. Sol. Energy **114**, 32–38 (2015)
2. A. Nevosad et al., Micro four-point probe investigation of individual ZnO grain boundaries in a varistor ceramic. J. Eur. Ceram. Soc. **34**, 1960–1970 (2014)
3. F. Lei et al., Hydrothermal synthesis and photovoltaic properties of ZnO particles and their application in TiO_2/ZnO-based dye-sensitized solar cells. J. Chin. Ceram. Soc. **41**, 12–18 (2013)
4. D. Liu, et al. Perovskite solar cells with a planar heterojunction structure prepared using room-temperature solution processing techniques. Nat. Photonics. **342** (2013)

5. Y. Hong, C.G. Tian, B.J. Jiang et al., Facile synthesis of sheet-like ZnO assembly composed of small ZnO particles for highly efficient photocatalysis. J. Mater. Chem. A **1**, 5700–5708 (2013)
6. K. Sambath, M. Saroja, M. Venkatachalam et al., Morphology controlled synthesis of ZnO nanostructures by varying pH. J. Mater. Sci.: Mater. Electron. **23**, 431–436 (2012)
7. Q. Ma, Y. Wang et al., Controllable synthesis of hierarchical flower-likeZnO nanostructures assembled by nanosheets and its optical properties. Superlattices Microstruct. **84**, 1–12 (2015)
8. J. JXu et al., Application of ZnO micro-flowers as scattering layer for ZnO-based dye-sensitized solar cells with enhanced conversion efficiency. Sol. Energy **101**, 150–159 (2014)
9. A. Jana et al., A comparative study on the dye sensitized solar cell performance of solution processed ZnO. Sol. Energy **102**, 143–151 (2014)
10. Y.H. Ko, J.S. Yu, Tunable growth of urchin-shaped ZnO nanostructures on patterned transparent substrates. Cryst EngComm **14**, 5824–5829 (2012)
11. X. Wang, H.B. Fu, A.D. Peng et al., One-pot solution synthesis of cubic cobalt nanoskeletons. Adv. Mater. **21**, 1636–1640 (2009)
12. S. Xu, Y. Ding, Y.G. Wei et al., Patterned growth of horizontal ZnO nanowire arrays. J. Am. Chem. Soc. **131**, 6670–6671 (2009)
13. D. Barreca, D. Bekermann, A. Devi et al., Novel insight into the alignment and structural ordering of supported ZnO nanorods. Chem. Phys. Lerres **500**, 287–290 (2010)
14. C.Y. Lin, Y.H. Lai, H.W. Chen et al., Highly efficient dye-sensitized solar cell with a ZnO nanosheet-based photoanode. Energy Environ. Sci. **4**, 3448–3455 (2011)
15. J. Demel, J. Pleštil, P. Bezdička et al., Layered zinc hydroxide salts: delamination, preferred orientation of hydroxide lamellae, and formation of ZnO nanodiscs. J. Colloid Interface Sci. **360**, 532–539 (2011)
16. S. Cheng, D. Yan, J.T. Chen et al., Soft-template synthesis and characterization of ZnO_2 and ZnO Hollow Spheres. J. Phys. Chem. C **113**, 13630–13635 (2009)
17. H. Lu, B. Dong, L. Zhao et al., ZnO nanosheet-based hierarchical microarchitectures for enhanced conversion efficiency in dye-sensitized solar cells. J. Mater. Sci.: Mater. Electron. **23**, 1905–1909 (2012)
18. C.S. Liu, Y. Masuda, Y.Y. Wu et al., A simple route for growing thin films of uniform ZnO nanorod arrays on functionalized Si surfaces. Thin Solid Films **503**, 110–114 (2006)
19. S. Suwanboon, P. Amornpitoksuk, A. Sukolrat, Dependence of optical properties on doping metal, crystallite size and defect concentration of M-doped ZnO nanopowders(M = Al, Mg, Ti). Ceram. Int. **37**, 1359–1365 (2011)
20. K. Hirota, M. Sugimoto, M. Kato et al., Preparation of zinc oxide ceramics with a sustainable antibacterial activity under dark conditions. Ceram. Int. **36**, 497–506 (2010)
21. C. Cheng et al., Three dimensional urchin-like ordered hollow TiO_2/ZnO nanorods structure as efficient photoelectrochemical anode. Nano Energy **2**, 779–786 (2013)
22. Y. Zhou, M.Y. Li et al., Synthesis of sea urchin-like ZnO by a simple soft template method and its photoelectric properties. Mater. Sci. Semicond. Process. **27**, 1050–1056 (2014)
23. Y. Zhou, D. Li, Y. Huang et al., Effect of KOH treatment on structural and photovoltaic properties of ZnO nanorod arrays. Trans. Nonferrous Met. Soc. China **22**, 2736–2741 (2012)
24. I. Beinik, M. Kratzer, A. Wachauer et al., Electrical properties of ZnO nanorods studied by conductive atomic force microscopy. J. Appl. Phys. **110**, 052005 (2011)
25. G. Brauer, W. Anwand, D. Grambole et al., Non-destructive characterization of vertical ZnO nanowire arrays by slow positron implantation spectroscopy, atomic force microscopy, and nuclear reaction analysis. Nanotechnology **18**, 195301 (2007)
26. L. Zheng, Y. Ma et al., Improved light absorption and charge transport for perovskite solar cells with rough interfaces by sequential deposition. Nanoscale **6**, 8171–8176 (2014)